Research Square

Preprints are preliminary reports that have not undergone peer review.
They should not be considered conclusive, used to inform clinical practice,
or referenced by the media as validated information.

Feasibility of Diffuse Reflectance Spectroscopy for Distal Margin Assessment in Colorectal Cancer Surgery

Joris T. Hepkema

j.hepkema@nki.nl

Netherlands Cancer Institute - Antoni van Leeuwenhoek Hospital

Isis Boeije

Delft University of Technology

Arend G.J. Aalbers

Antoni van Leeuwenhoek Hospital

Brechtje A. Grotenhuis

Antoni van Leeuwenhoek Hospital

Marinke Westerterp

Antoni van Leeuwenhoek Hospital

Freija Geldof

Netherlands Cancer Institute - Antoni van Leeuwenhoek Hospital

Behdad Dashtbozorg

Netherlands Cancer Institute - Antoni van Leeuwenhoek Hospital

Theo J.M. Ruers

Netherlands Cancer Institute - Antoni van Leeuwenhoek Hospital

Article

Keywords:

Posted Date: June 29th, 2026

DOI: https://doi.org/10.21203/rs.3.rs-9979155/v1

License: This work is licensed under a Creative Commons Attribution 4.0 International License.
Read Full License

Additional Declarations: No competing interests reported.

Version of Record: A version of this preprint was published at Scientific Reports on October 16th, 2026. See the published version at https://doi.org/10.1038/s41598-026-75555-4.

Feasibility of Diffuse Reflectance Spectroscopy for Distal Margin Assessment in Colorectal Cancer Surgery

Joris T. Hepkema[1,*], Isis Boeije[2], Arend G.J. Aalbers[3], Brechtje A. Grotenhuis[3], Marinke Westerterp[3], Freija Geldof[1], Behdad Dashtbozorg[1], and Theo J.M. Ruers[1]

[1]Image-Guided Surgery, Netherlands Cancer Institute - Antoni van Leeuwenhoek Hospital, Amsterdam, 1066 CX, the Netherlands
[2]Technical Medicine, Technical University Delft, 2628 CD, the Netherlands
[3]Surgical Oncology Department, Antoni van Leeuwenhoek Hospital, Amsterdam, 1066 CX, the Netherlands
[*]j.hepkema@nki.nl

ABSTRACT

Adequate distal resection margins (DRM) in colorectal cancer surgery are critical for oncological safety while preserving sphincter function. Current intra-operative DRM assessment methods are limited or have major drawbacks, leaving surgeons without real-time guidance. Diffuse reflectance spectroscopy (DRS) offers a potential solution using rapid optical feedback on tissue characteristics. In this study, continuous measurements were performed on freshly excised colorectal specimens using a broadband DRS system (400–1600 nm). A binary classification approach was applied to discriminate between healthy and tumor locations. Multiple feature extraction strategies were evaluated in combination with different classifiers and hyperparameter tuning was performed. A total of 39,741 spectra (22,451 non-tumor, 17,290 tumor) from 86 patients were included. Using the first derivative of the spectra paired with a radial basis function (RBF) support vector machine achieved the best results, reaching a mean Matthews Correlation Coefficient (MCC) of 0.820 ± 0.015. Sensitivity and specificity were 0.888 ± 0.015 and 0.928 ± 0.028, respectively. This study demonstrates the feasibility of using DRS combined with machine learning to distinguish tumor from non-tumor regions in colorectal cancer surgery. Future work should focus on prospective validation of distal margin assessment and exploring probe designs with deeper penetration to enhance intra-operative applicability.

Introduction

Colorectal cancer accounts for 9.5% of all newly diagnosed cancers in the Netherlands in 2023[1] and accounts for 7.8% of all new cancer cases worldwide[2]. It is the 3^{rd} most prevalent cancer among males worldwide[3], and the number of colorectal cancer cases is predicted to increase to 3.2 million new cases and 1.6 million deaths by 2040[4].

In rectal cancer surgery (total mesorectal excision), the circumferential resection margin (CRM) and distal resection margin (DRM) are known to be strong predictors for local tumor recurrence and thus for the success of surgical resection (Figure 1)[5]. The need for an adequate DRM was recently highlighted in exploratory analysis of the RAPIDO trial, which found a DRM length of $\leq$ 10 mm to be significantly associated with a markedly higher 8-year locoregional recurrence rate in patients who underwent total neoadjuvant treatment (TNT)[6]. The optimal surgical resection strikes a balance between the length of the residual rectum stump (and thus of complaints and impact on quality of life) on one hand[7–13], and the optimal DRM for oncologic safety on the other[6,14–18]. Intra-operative guidance for DRM assessment could assist surgeons in balancing oncological safety against sphincter preservation, particularly in low rectal tumors where every millimeter of distal bowel length may influence functional outcomes and the feasibility of restorative surgery.

Due to lack of tactile feedback, localization of the distal tumor boundaries can be challenging during laparoscopic or robot-assisted procedures. To allow surgeons to localize the tumor intra-operatively during these procedures, tattoo ink can be applied endoscopically before surgery[19,20]. However, use of this tattoo ink has some controversy due to reported adverse events[21,22]. Furthermore, the accuracy has been reported to be as low as 69%[23] due to spreading of the ink outside of the desired area, which can lead to wider DRM without oncological benefit. During surgery, frozen section of a suspect margin can be performed to assess potentially irradical margins[24]. This is currently the golden standard for intra-operative margin assessment, but is known to have drawbacks; it is a time-consuming process[25]; it can miss more distal spread of a tumor after chemoradiation, due to fragmentation of the lesion[26,27]; and the application is largely based on surgeon preference[28]. Intra-operative guidance for DRM assessment can be of help to determine the optimal DRM[29].

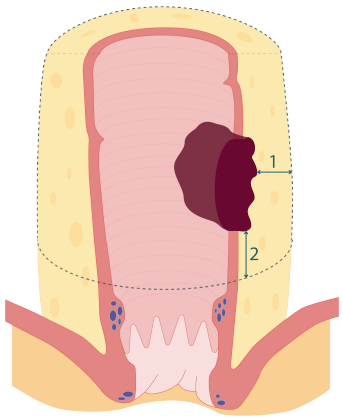


Figure 1. Schematic overview of the resection margins in surgery of the rectum. Dashed lines: resection margins; 1: Circumferential margin; 2: Distal resection margin.

In the field of surgical oncology, several new techniques have been developed for better surgical margin assessment during surgery such as (3D) ultrasound[30–41], Fourier transform infrared spectroscopy[42], Raman spectroscopy[43], optical coherence tomography[44], fluorescence agents[45], rapid evaporative ionization mass spectrometry[46], flow cytometry[47], navigation[48] and diffuse reflectance spectroscopy (DRS). DRS has shown potential to distinguish malignant tissue from healthy tissue and to predict positive surgical resection margins over multiple types of cancer[49], including breast cancer[50,51], soft-tissue sarcomas[52], liver tumors and metastases[53], oral cancer[54], lung tumors[55], prostate cancer[56,57] and colorectal cancer[58–65]. DRS has advantages over other techniques, namely (1) it does not require any contrast agent or placement of foreign bodies, (2) measurements are done using harmless light without the need for removal of the measured tissue for classification, and (3) can be conducted in real-time with the right set-up.

Most of the previous colorectal DRS studies have primarily focused on assessing the CRM[58,61–63,65] or used either sliced tissue[60,66] or endoscopic measurements[59,64,67]. In addition, measurements have largely been point-based, sampling a small area at a time. This method carries a few downsides; due to the small size of the sampled location, there is an inherent risk of undersampling. Furthermore, these point measurements can take up to 15 seconds for one measurement location, making live clinical use virtually impossible. Saito Nogueira et al. mention real-time measurements with a single reading of about 2-3 seconds[64]. While this is a huge step forward, scanning an entire specimen surface or even a reasonably sized area of interest would still take up too much time for intra-operative use. Nazarian et al. performed real-time classification of tumor and non-tumor tissue in colorectal cancer using DRS, with an accuracy of 90.8% for distinguishing tumor measurements from healthy colon measurements, excluding measurements of fibrosis[63]. Where they mainly focused on assessing the CRM, this study aims to validate DRS for DRM assessment.

To address the aforementioned opportunities for improvement, this study investigates whether DRS can be used to determine the localization of tumor tissue, with the goal of determining the edge of the tumor and thus the DRM. In clinical practice, tissue is often heterogeneous, with healthy tissue layers potentially overlying deeper tumor. The ability of DRS to detect such inhomogeneous structures and still identify tumor presence would be highly valuable for intra-operative guidance. Therefore, this research focuses on assessing whether DRS can reliably distinguish tumor presence and thus inform the optimal distal dissection location in colorectal surgeries. To achieve this goal, we make use of continuous DRS measurements, allowing rapid acquisition of data across the bowel surface.

The main contribution of this work can be summarized as:

- Prospective creation of a dataset containing continuous DRS measurements across tumor and healthy regions on freshly excised colorectal cancer specimens
- Training and validating a robust machine learning model for tumor location detection using the weakly labeled acquired data
- Achieving a prospective proof-of-concept using the trained model to detect the tumor boundary in real-time

Materials and methods

Diffuse reflectance spectroscopy system

The DRS system used in this study consisted of a laser light source (SuperK Compact White Light Laser, NKT Photonics, Birkerød, Denmark; 450–2400 nm) and two spectrometers. The first spectrometer covered the visible wavelength range (AVASPEC-HS2048XL-EVO, 200–1160 nm), while the second covered the near-infrared range (AVASPECNIR256-1.7-RS,

900–1750 nm). The handheld fiber-optic probe included two fibers with a source-to-detector distance (SDD) of 2 mm. All components were controlled using in-house developed MATLAB software.

Conventional approaches acquire a single spectrum per location, using a broadband halogen light source. In contrast, our system makes use of a laser, allowing it to be operated in continuous fashion and performing 5 to 8 measurements per second. By capturing this continuous stream of spectra rather than isolated snapshots, the system enables rapid sampling of substantially larger areas of the resection surface, thereby capturing a broader range of spectral variations and more closely reflecting real-time intra-operative resection surface screening.

Patient inclusion

Patients were included prospectively at the Netherlands Cancer Institute (NKI-AvL). Patients diagnosed with colorectal cancer and undergoing surgical resection at the NKI-AvL hospital were eligible. Patients with at least T3 tumors on pre-operative imaging were included. This study is approved by the Netherlands Cancer Institute - Antoni van Leeuwenhoek Hospital Institutional Review Board (IRBdm23-075) and adheres to the Declaration of Helsinki. Hospital general informed consent was obtained from all patients and/or their legal guardians in accordance with the Dutch Medical Research Involving Human Subjects Act (WMO), allowing the use of their biological materials and data in this study.

Measurement protocol

This study was conducted *ex vivo*. Directly after removal by the surgeon, the specimen was taken to our measurement setup and measurements were performed without modification of the tissue. The colorectal tumor location on the specimen was identified by inspection, palpation and ultrasound assessment. Colorectal tumor measurements were performed over the gross tumor location. Non-tumor (healthy) measurements were obtained from healthy colon or rectal wall and adipose tissue located at least 1 cm away from the identified colorectal tumor region. To ensure an adequate representation of tissue heterogeneity, multiple DRS measurements were performed on a larger area rather than at a single point. The number of measurements depended on the tumor- and specimen size, but typically varied from 600-1000 measurements per patient, over an area of one by one centimeter for colorectal tumor area and five by five centimeter for non-tumor tissue.

We used the acquired spectra for training a model to distinguish colorectal tumor tissue from non-tumor tissue. Ideally, measurements would be taken over the colorectal tumor and distally from the colorectal tumor, to get data for both tissue types. However, as surgeons try to keep DRM minimal where possible, most specimens did not have enough space distally of the gross colorectal tumor to carry out measurements. We carried out healthy measurements over healthy tissue proximal to the colorectal tumor, as we do not expect a difference in optical fingerprint.

After data collection, the measured colorectal tumor region was marked with ink to allow histopathologic correlation. Since healthy tissue was measured at least 1 cm away from the colorectal tumor region and is clearly distinguishable with ultrasound imaging, no ink marking was placed here. After the data acquisition, all specimens were returned to the Pathology Department for histopathologic processing following standard clinical procedure.

Data preprocessing

Prior to performing the measurements, a calibration was performed, as described earlier by Geldof et al.[52]. Briefly, dark reference spectra were acquired with the light source switched off to correct for ambient light and dark current noise, while white reference spectra were obtained using a Spectralon reflectance standard (WS-2, Avantes, Apeldoorn, the Netherlands) to correct for the spectral response of the lamp and the system sensitivity. The spectra from the visible and near-infrared spectrometers were stitched together by the DRS software to create a continuous spectrum ranging from 400 to 1600 nm. Due to the resolution of these spectrometers, the final dataset contained 356 spectral bands, each band having a range of 3.37 nm. To compensate for intensity variations caused by differences in probe pressure or environmental conditions, the spectra were normalized using standard normal variate (SNV) normalization. With SNV normalization, the mean is subtracted from the spectrum, after which the result is divided by the standard deviation of the spectrum.

Data labeling

Spectra were labeled as colorectal tumor whenever colorectal tumor tissue was present at the measurement location at histopathologic analysis, irrespective of its depth. The other measurements were labeled as non-tumor. The histological analysis served as the ground truth for labeling the DRS spectra as colorectal tumor or non-tumor tissue; locations that were thought to be colorectal tumor locations that ended up not containing tumor after histopathologic analysis were excluded. Healthy measurements from these patients were included in the non-tumor dataset.

Data analysis

Multiple supervised classification algorithms were developed and assessed, in combination with various feature selection strategies, to determine the optimal model for accurately detecting colorectal tumor locations. The input to the algorithms

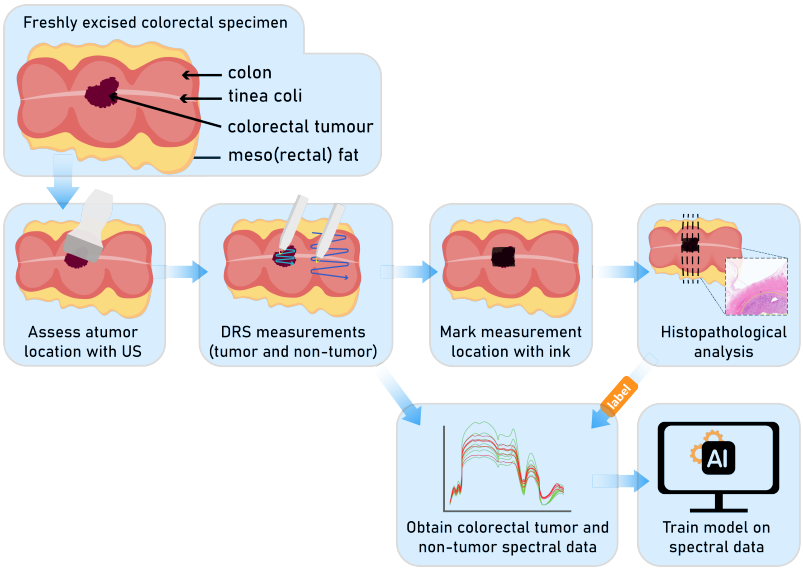


Figure 2. Flowchart showing the measurement protocol. First, the location of the colorectal tumor is assessed on the freshly excised specimen. Next, colorectal tumor and non-tumor DRS measurements are obtained. The measured colorectal tumor location is inked to correlate histopathologic analysis, from which we obtain labels for the acquired data. Lastly, this data is used for training a machine learning model.

consisted of the SNV-normalized DRS spectra and the ground truth tissue-type was used as label. All data was split into a training/validation dataset (80% of data) and a test set (20%). The model selection was performed on the training/validation dataset only, while hyperparameter tuning was performed on the training/validation and subsequently tested on the test dataset for assessing performance. Data was split patient-wise to prevent data leakage between the training/validation and the test datasets. During training, data was balanced using a synthetic minority oversampling technique (SMOTE), as recommended for DRS in optical diagnosis[49], implemented through imbalanced-learn[68,69]. Briefly, SMOTE creates synthetic observations by interpolating between random observations in the minority class and k of its nearest neighbors. We balanced the tumor and non-tumor classes by applying SMOTE with $k = 7$ for all models mentioned hereafter.

Classifier & Feature Selection Method Combination Comparison

We assessed five feature selection/generation methods (FSM) in combination with five classification models to find the optimal combination for this task. The following FSM were assessed:

A) Using the full spectra directly (no FSM applied).
B) The first derivative of the full spectra to enhance subtle spectral variations.
C) Least Absolute Shrinkage and Selection Operator (LASSO) regression, a linear method with L1 regularization that penalizes feature coefficients. Less informative coefficients are reduced to zero. A grid search over regularization parameters (c = 0.1–1) was used and evaluated based on classification accuracy.
D) Linear Discriminant Analysis (LDA) was used as a feature-ranking approach. LDA is a supervised linear method that finds combinations of features maximizing between-class separation relative to within-class variance. LDA was fitted to the full feature set, and the absolute values of the resulting discriminant coefficients were used to rank features. The 100 highest-ranking original features were retained for subsequent analysis.
E) k-means spectral band features, where ten wavelength bands were clustered based on spectral intensity similarity and the mean intensity of each band was used as a feature.

These feature generation and selection methods were partly chosen because other similar research investigated these methods, showing promising classification possibilities[65,70]. Additional feature generation methods were added based on their eligibility for our purposes.

The selected FSM were combined with the following classifiers:

A) A basic Linear Support Vector Machine (SVM).
B) A polynomial SVM with $degree = 2$ and $C = 1$.
C) A radial basis function (RBF) SVM with $C = 1$ and $gamma = scale$.
D) A multi-layer perceptron (MLP) with the hidden layers sizes set to $\frac{1}{2}$ and $\frac{1}{4}$ of the amount of features used as model input.
E) A Random Forest classifier with 100 estimators.

If not mentioned, default parameter values were used for these classifiers. These particular models were selected because earlier research used similar models for DRS data classification and showed high classification performance[65,66,70]. The combinations of each FSM with each classifier were assessed using five-fold cross-validation. Stratification preserved the class balance in all folds, and samples from the same patient were never in both the training and validation sets to prevent patient data leakage. Data and corresponding predictions were concatenated over five folds, after which the following performance metrics were calculated over all five folds: Area Under the Receiver Operating Characteristic curve (AUROC), sensitivity, specificity, accuracy, and the Matthews correlation coefficient (MCC). MCC ranges between -1 and 1 and provides a robust measure that only provides a high score if predictions have both high rates of true positives/negatives, but also low rates of false positives/negatives. Using the results of these tests, we chose the best performing FSM and classifier combination, based primarily on the achieved MCC, as achieving a balance between sensitivity and specificity was considered most important.

Hyperparameter Tuning and performance evaluation on Test Data

A manual grid search was performed on the highest scoring model + FSM combination for hyperparameter tuning. We tested all possible (twenty) combinations of C (0.1, 1, 10, 100) and gamma (0.01, 0.1, 1, 10, 'scale'). For each combination, the model was trained and evaluated on the same metrics as mentioned before. With the result of this grid search, an optimal combination of the hyperparameters was selected based on the validation MCC. A model was subsequently trained on all training and validation data together, using these optimal hyperparameters. This model was then used to predict on the separate test set, and the same performance metrics were assessed. To ensure the robustness of this approach, hyperparameter grid search was repeated tenfold, with a different distribution of patients for every iteration. The final metrics are those of the ten iterations combined, as well as the combination of hyperparameters used.

Prospective testing on fresh colorectal specimens

The final model, selected based on performance metrics over all ten iterations, was tested as a proof-of-concept. Each measurement was directly used for predicting the label - colorectal tumor or non-tumor - and feedback was provided by using an audible signal with a changing pitch, based on the prediction. Using this, linear measurements were performed over three freshly excised rectal cancer specimens. As most freshly excised specimens have a very limited DRM, we simulated performing DRM measurements by assessing the proximal boundary of the colorectal tumor, instead, as no differences in tissue composition are to be expected between the proximal and distal boundaries. At a location where a clear change in pitch/predicted label was observed, a suture was placed to mark the predicted border of the colorectal tumor. Afterwards, during preparation for histopathologic analysis, we analyzed the distance from the actual macroscopic colorectal tumor area to the placed suture to assess the accuracy of this method.

Results

Patient characteristics

Freshly excised colorectal specimen from 86 patients were included in this study (Table 1). Half of patients did not receive neo-adjuvant treatment (n=46, 53%), while 18 (21%) received chemotherapy, 2 received radiotherapy (2%), 4 received immunotherapy (5%) and 16 received both chemotherapy and radiotherapy (19%). Out of the pretreated patients, most showed a mix of residual colorectal tumor tissue with fibrosis (TRG 3-4, n=30, 75% of pretreated patients). While most of the included patients had a malignancy of the sigmoid (n=22, 26%) or rectum (n=26, 30%), patients with colorectal tumors of all parts of the large bowel (colon, sigmoid and rectum) were included. One patient (1%) did not show any residual colorectal tumor after histopathologic analysis (pT0). The majority of patients had low grade adenocarcinomas (n=60, 70%). As an expected result of measuring colorectal tumors visible on ultrasound imaging with a reasonable proximity to the resection margins, most patients had a pT stage of 3 or higher (n=76, 88%). Two patients (2%) were found to have had a peritoneal metastasis instead of a primary colorectal tumor in the bowel wall after histopathologic analysis. One patient (1%) had no mention of the TRG; this was one patient with the peritoneal metastasis. For these two patients, colorectal tumor measurements were excluded, but their non-tumor measurements were used.

Data characteristics

Saturated spectra were removed from the dataset, to ensure that only high-quality spectra were used for the analysis. After this, a total of 39,741 diffuse reflectance spectra were used, out of which 22,451 were labeled as non-tumor and 17,290 as colorectal tumor. The mean and standard deviations of DRS spectra of the non-tumor and colorectal tumor labels are shown in Figure 3.

Prediction Model & Feature Selection Method Combination Comparison

Results per combination of FSM and classifier can be found in Table 2. Comparing performance based on MCC, using the 1st derivative of the data as an input combined with either a polynomial SVM (MCC=0.78) or an RBF SVM (MCC=0.78) showed

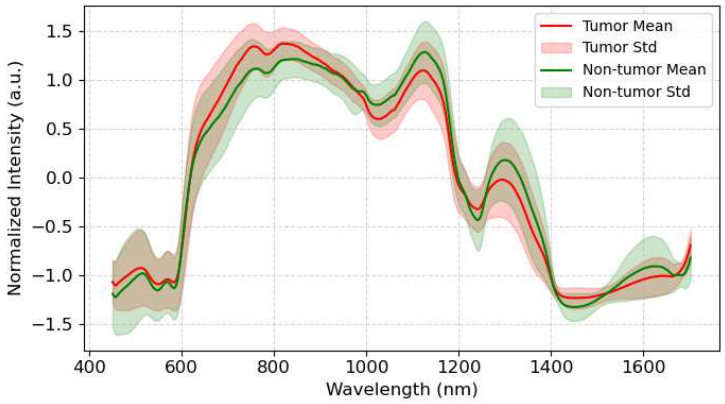


Figure 3. Mean spectra per tissue type, over all patients.

the best performance. Out of all prediction models, the Random Forest showed the lowest MCC values (MCC: 0.67-0.74) across all FSM, while polynomial SVM or RBF SVM (for both, MCC: 0.68-0.78) performed best. Regarding FSM, *k*-means spectral bands performed worst (MCC: 0.64-0.68) while the first derivative performed best (MCC: 0.73-0.78).

Similar trends can be seen for the other performance metrics. Overall, the use of the first derivative consistently resulted in the highest sensitivity, specificity, accuracy, and AUROC, particularly when combined with either a polynomial or an RBF SVM. Both resulted in a sensitivity of 0.89, specificity of 0.90, accuracy of 0.89, and an AUROC of 0.95. While both SVM variants showed comparable performance for first-derivative features, the RBF SVM demonstrated slightly better performance across the remaining FSMs and metrics. Therefore, the RBF SVM was selected for subsequent analysis.

Hyperparameter Tuning and Validation on Test Data

Model optimization with hyperparameter tuning was conducted for the RBF SVM with the first derivative of the spectra. For an RBF SVM, C controls the trade-off between achieving a smooth decision boundary and correctly classifying training points, with higher C values giving more complex boundaries. Gamma defines how far the influence of a single training example reaches; higher values mean each point influences only its close neighbors, with more risk of overfitting. A scaled gamma adapts the value to the dataset's variance and dimensionality by taking the inverse of the product of the number of features and the variance of the dataset[71]. A manual grid search was conducted for combinations of C and gamma, where C values were [0.1, 1, 10, 100] and gamma values were [0.01, 0.1, 1, 10, 'scale']. Performance metrics over all ten iterations can be seen in Figure 4.

Over all hyperparameter combinations and over the ten iterations with different patient splits, the best performing C/gamma combination was found to be (C=1, gamma=10) in 3 iterations (mean MCC: 0.82 ± 0.015); (C=10, gamma='scale') in 3 iterations (MCC: 0.71 ± 0.099); (C=10, gamma=1) in 2 iterations (MCC: 0.81 ± 0.016); (C=100, gamma=1) in 1 iteration (MCC: 0.76) and (C=1, gamma='scale') in 1 iteration (MCC: 0.65). The median test MCC over all ten iterations was 0.80, with a mean of 0.76 and a standard deviation of 0.079.

The ROC curve can be seen in Figure 4, which includes the golden standard (frozen section) for comparison. Using Youden's J statistic, the optimal threshold was found, resulting in a sensitivity of 0.93 and specificity of 0.91 for a threshold of 0.62. Using an adjusted cutoff optimized for specificity while maintaining the same sensitivity as frozen section, a specificity of 0.95 was found for a threshold of 0.86.

Prospective testing on fresh colorectal specimens

Using the selected optimal model architecture, a final model was trained on all data (training, validation and testing). The predictions made using this model can be seen in Figure 5. As the bowel wall is mobile, exact measurement of the distance from suture location to the gross colorectal tumor edge was not possible. However, as Figure 5 shows, the predicted colorectal tumor boundary was very accurate, showing a clear potential benefit for surgeries in which tactile feedback is not an option.

Discussion

This study explored the feasibility of using DRS for real-time classification of colorectal tumor versus non-tumor tissue, with the aim of supporting intra-operative decision making regarding distal resection margins during (minimally invasive) colorectal cancer surgery. Ultimately, the clinical value of such a system lies in its ability to assist surgeons in identifying the distal extent

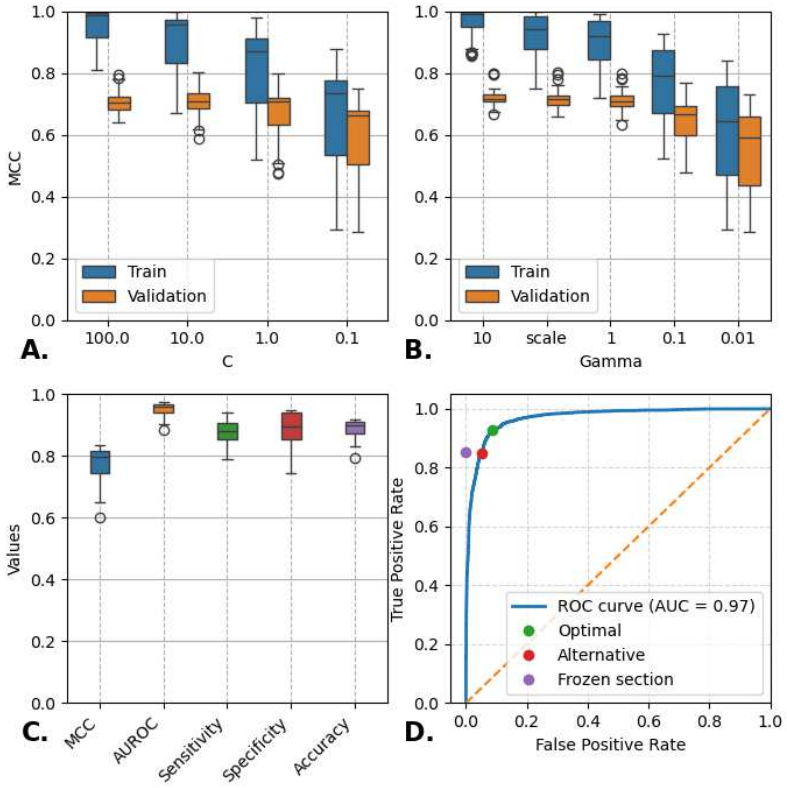


Figure 4. Graphs with main results of hyperparameter tuning and crossvalidation folds. (**A**) Influence of C on MCC over ten iterations of training and validation datasets. (**B**) Influence of gamma on MCC over ten iterations of training and validation datasets. (**C**) Performance metrics for the test sets across all ten iterations with different patient splits. (**D**) ROC curve showing performance metrics for the final model. The metrics for frozen section can be seen in the plot (purple, sensitivity = 0.85, specificity = 1.00), as well as the optimal point calculated using Youden's J statistic (green, sensitivity = 0.93, specificity = 0.91) and when aiming for the same sensitivity as frozen section (red, specificity = 0.95).

of the tumor and selecting an oncologically safe transection level while avoiding unnecessary sacrifice of healthy bowel. By performing rapid measurements (5-8 per second) and labeling all measurements taken within histopathologically confirmed tumor regions as "colorectal tumor" — regardless of depth — and those outside as "non-tumor" (including both adipose and muscle tissue), we created a large dataset. Next, we followed a systematic approach to develop a classification algorithm, trying various feature selection methods combined with different classification models. Ultimately, we used the best performing combination and fine-tuned this through a hyperparameter grid search over ten iterations with different patient splits, to make sure our results were robust.

Feature Selection/Extraction Methods

Compared with using the whole spectra for analysis, using the first derivative of the spectra gave higher performance in four out of five classification models; only a Linear SVM performed slightly better when using the whole spectra (MCC=0.75 vs 0.73, Table 2). Applying this feature extraction method reduces noise while enhancing subtle spectral variations. Additionally, computing the first derivative emphasizes local changes in spectral intensity rather than absolute values, which can enhance subtle differences between tumor and non-tumor tissue that might otherwise be missed. Multicollinearity (the number of highly correlated features) is also reduced, as adjacent wavelengths may show more contrast in the first derivative than in the original data.

While the other FSM were either expected to perform well, or performed well in earlier studies[70], none reached the same performance as using the first derivative of the data.

Classification Models

This study explored multiple SVM kernels: linear, polynomial and RBF. A linear SVM finds a straight hyperplane best separating classes, which performs best when the main differences between classes are captured by linear combinations of

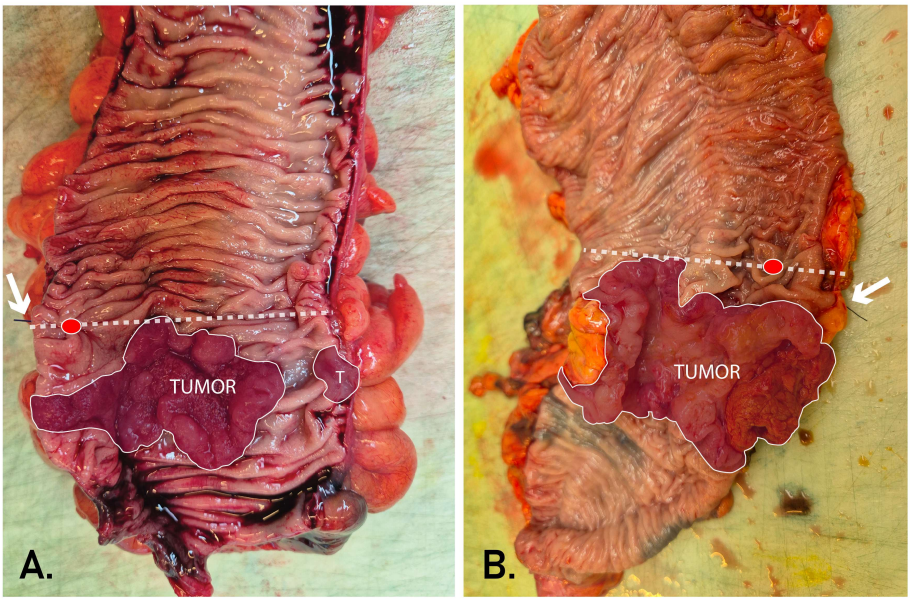


Figure 5. Results of prospective testing on 2 freshly excised colorectal specimen. (**A**) First specimen containing colorectal cancer (white border, purple area), cut open longitudinally. A suture (red dot, white arrow) marks the location of the predicted colorectal tumor border (dashed white line). (**B**) Second specimen containing colorectal cancer (white border, purple area), cut open longitudinally. A suture (red dot, white arrow) marks the location of the predicted colorectal tumor border (dashed white line).

wavelengths. A polynomial SVM fits a globally curved decision boundary, modeling interactions between features. An RBF SVM maps the data into a high-dimensional space using a Gaussian kernel, which can capture more subtle differences between classes. In this study, an RBF SVM achieved the best results. This is to be expected, as it is better poised to distinguish more complex differences between colorectal tumor and non-tumor spectra. An MLP achieved similar results, but failed to reach the same predictive strength. A Random Forest classifier performed worst, showing it may not be able to capture the more complex differences.

Iterative Grid Search for Hyperparameter Tuning

We used the first derivative of the spectral data as input features, and an RBF SVM prediction model with (C=1, gamma=10) for the iterative grid search. Using this setup, a mean test MCC of 0.82 ± 0.015 was achieved. This combination of hyperparameter values was the best performing over three of ten iterations, followed closely by (C=10, gamma='scale') with a mean MCC of 0.71 ± 0.099, also performing best over three iterations. Of these two, the first combination both achieves a higher mean MCC and a smaller standard deviation, showing a more robust model than the second combination. This is reflected in the sensitivity and specificity, too; (C=1, gamma=10) reaches a sensitivity and specificity of 0.89 ± 0.049 and 0.93 ± 0.028, respectively.

The grid search revealed clear trends in how hyperparameter combinations affect model performance (Figure 4). For lower gamma values (0.01 and 0.1), increasing the value of C consistently led to higher accuracy and MCC scores. This shows the role of C as a regularization parameter: larger values of C penalize misclassifications more strongly, encouraging the model to fit the training data more closely. At low gamma values, the decision boundary remains relatively smooth, so increasing C improves performance without introducing instability. However, at gamma = 1, 10 and scaled, the performance trend changes. Accuracy and MCC plateaus or decrease when the C value was increased. This suggests that the combination of high C and high gamma produces an overly complex model with high variance. Larger gamma values make the decision boundary more sensitive to local variations, while smaller gamma values produce smoother boundaries. When both C and gamma are large, the model becomes highly flexible, fitting noise in the training data and thus overfitting on the training data. Intermediate gamma values (1 and scale) performed best, suggesting an optimal balance between model complexity and generalization, if combined with a fitting regularization parameter.

Comparison with other studies

Several other studies have investigated the use of DRS for colorectal cancer (CRC) classification earlier[59,61,62,67,72], but none with the explicit goal of assessing the DRM. Saito Nogueira et al.[62] reported strong diagnostic performance for distinguishing

colorectal tumor and non-tumor tissue, with sensitivities over 0.96 and specificities of 0.99 in two probe designs. These results are comparable to ours, while the study designs differ on a few points. Firstly, they removed stool and blood from the specimen, whereas we did not. Secondly, they applied spectral fitting to estimate biomolecule concentrations, instead of directly using (a derivative of) the measured spectra, with the risk of making inaccurate assumptions about tissue composition. Finally, this study had a larger dataset with diverse colorectal tumor types and localizations, which supports the development of a more robust and clinically representative classification model.

Other recent studies also reached promising results using DRS[59,67]; however, their measurements were conducted on the luminal surface of the bowel. Their results are not expected to translate well to our research, as the added tissue layer over the colorectal tumor makes classification a harder task.

Other previous work has shown that distinguishing vital colorectal tumor tissue from fibrosis using DRS is feasible in homogeneous tissue, with reported accuracies up to 0.88, but performance decreases markedly in the presence of mixed tissue[58]. In the current study, tissue heterogeneity was not explicitly quantified; however, 36 patients exhibited partial (TRG 2–4) or complete (TRG 1) response to neoadjuvant therapy, making the presence of mixed tumor–fibrotic tissue likely. A brief analysis on 50 out of 404 pathology slides used for this study by our pathologist confirmed that in this subset, some amount of fibrosis was present in every slide. The fact that this study was not hindered by the presence of this fibrosis may be attributed to the smaller sample size of our earlier study (38 patients/117 measurements versus 86 patients/39,741 measurements). Future work should further investigate the influence of fibrosis on DRS-based classification.

When compared to alternative intra-operative techniques, ultrasonography has been explored for distal resection margin assessment in rectal cancer[30,32]. While promising, Giuliani et al. did not report diagnostic performance metrics, precluding direct comparison. Ultrasound may offer complementary structural information, but further quantitative evaluations are needed to establish its role in margin assessment.

Frozen section analysis remains the clinical reference standard for intra-operative margin evaluation, with reported sensitivities of 85.2% and specificities of 100% for predicting positive margins in rectal cancer[28]. Although the specificity of frozen section was not matched by the current model at the default operating point, the classification threshold of the DRS-based approach can be adjusted along the ROC curve to prioritize either sensitivity or specificity, resulting in a specificity of 0.95 with the same sensitivity as frozen section (Figure 4). As mentioned before, frozen section adds a substantial amount of time to the surgical procedure[25], while DRS techniques have the advantage of giving near-instant results. This allows for quicker sampling (and re-sampling) of a large area of the area of interest. Going over the same spot multiple times with the probe may allow for even more accurate predictions, as the surgeon can use multiple predictions per location to see if one positive was an outlier, or whether predictions are consistent.

Limitations and future directions

In this study, a DRS probe with an SDD of 2 mm was used, which corresponds to an approximate tissue sampling depth of 1-2 mm according to Monte Carlo simulations[54]. Colorectal tumors situated deeper than the effective sampling depth may show minimal or no colorectal tumor optical signs in the spectra, potentially leading to colorectal tumor tissue being misclassified as non-tumor. DRM assessment is especially challenging in those surgeries that are carried out either laparoscopically or robot-assisted, due to the lack of tactile feedback. As these techniques are mostly used in lower-stage colorectal tumors (T2-3), which do not or hardly grow beyond the colorectal wall, the colorectal tumor may be harder to detect with this probe design. For DRM assessment, deeper tissue penetration could therefore be preferable to minimize the risk of missing colorectal tumor presence . On the other hand, a larger SDD not only increases the depth measured, but also the lateral reach of the measurement, effectively lowering the resolution of the measurement. Furthermore, even with this simulated measuring depth in mind, we achieved a high accuracy, showing potential shortcomings of this theoretical modeling. Looking ahead, future research should validate the performance in stage T2 colorectal tumors specifically and explore the use of probes with larger and/or multiple SDD's to get a better idea of the sampling depth. Even so, it is good to note that, in laparoscopic and robot-assisted rectal surgery, the rectum is completely dissected from surrounding tissues at the location of planned transection. This means that access to the rectum is possible, and that measurement depth does not need to be much larger than in the current setup.

While the current study focused on tissue classification performance, future investigations should evaluate how accurately DRS can localize the histopathological tumor boundary in colorectal cancer and whether this information can influence surgical decision-making. Ultimately, the clinical relevance of DRS for distal margin assessment will depend not only on spectrum-level classification performance, but also on its ability to provide reliable guidance regarding the optimal distal transection site.

Conclusion

This study included 86 colorectal cancer patients, corresponding to nearly 40,000 measured DRS spectra. The trained classification models could accurately distinguish colorectal tumor from non-tumor regions, with the highest performance achieved using the first derivative of the spectra as input features for a RBF SVM classifier. These findings highlight the

potential of using DRS combined with selected machine learning techniques to provide real-time intra-operative guidance, making fast, intra-operative distal margin determination a possibility. Future research will focus on validating this technique prospectively in new patients, as well as seeking ways to further improve the deterministic accuracy of the model.

Data Availability

The datasets generated during and/or analyzed during the current study are available from the corresponding author on reasonable request.

References

1. Netherlands Comprehensive Cancer Organisation (IKNL), Netherlands Cancer Registry (NCR) Data | Incidence. Derived via nkr-cijfers.iknl.nl on 2025-03-13.
2. National Cancer Institute - Surveillance, Epidemiology, and End Results (SEER) Program. Cancer of the Colon and Rectum - Cancer Stat Facts. Derived via seer.cancer.gov/statfacts/html/colorect.html on 2025-03-13.
3. Wagle, N. S. *et al.* Cancer treatment and survivorship statistics, 2025. *CA: A Cancer J. for Clin.* **75**, 308–340, DOI: 10.3322/caac.70011 (2025). _eprint: https://acsjournals.onlinelibrary.wiley.com/doi/pdf/10.3322/caac.70011.
4. Morgan, E. *et al.* Global burden of colorectal cancer in 2020 and 2040: incidence and mortality estimates from GLOBOCAN. *Gut* **72**, 338–344, DOI: 10.1136/gutjnl-2022-327736 (2023).
5. Federatie Medisch Specialisten. Colorectaal carcinoom (CRC). Derived from https://richtlijnendatabase.nl/richtlijn/colorectaal_carcinoom_crc on 2026-01-13.
6. Prata, I. *et al.* Factors influencing locoregional recurrence rates in locally advanced rectal cancer after total neoadjuvant treatment versus chemoradiotherapy in the RAPIDO trial. *Br J Surg* **112**, znaf190, DOI: 10.1093/bjs/znaf190 (2025).
7. Martellucci, J. Low Anterior Resection Syndrome: A Treatment Algorithm. *Dis. Colon & Rectum* **59**, 79, DOI: 10.1097/DCR.0000000000000495 (2016).
8. Ekkarat, P., Boonpipattanapong, T., Tantiphlachiva, K. & Sangkhathat, S. Factors determining low anterior resection syndrome after rectal cancer resection: A study in Thai patients. *Asian J Surg* **39**, 225–231, DOI: 10.1016/j.asjsur.2015.07.003 (2016).
9. Carrillo, A. *et al.* Incidence and characterization of the anterior resection syndrome through the use of the LARS scale (low anterior resection score). *Cir Esp* **94**, 137–143, DOI: 10.1016/j.ciresp.2015.11.005 (2016).
10. Battersby, N. J. *et al.* Predicting the Risk of Bowel-Related Quality-of-Life Impairment After Restorative Resection for Rectal Cancer: A Multicenter Cross-Sectional Study. *Dis Colon Rectum* **59**, 270–280, DOI: 10.1097/DCR.0000000000000552 (2016).
11. Jimenez-Gomez, L. M. *et al.* Factors associated with low anterior resection syndrome after surgical treatment of rectal cancer. *Color. Dis* DOI: 10.1111/codi.13901 (2017).
12. Nguyen, T. H. & Chokshi, R. V. Low Anterior Resection Syndrome. *Curr Gastroenterol Rep* **22**, 48, DOI: 10.1007/s11894-020-00785-z (2020).
13. Bolton, W. S. *et al.* The Incidence of Low Anterior Resection Syndrome as Assessed in an International Randomized Controlled Trial (MRC/NIHR ROLARR). *Ann Surg* **274**, e1223–e1229, DOI: 10.1097/SLA.0000000000003806 (2021).
14. Zeng, W.-G., Liu, M.-J., Zhou, Z.-X. & Wang, Z.-J. A Distal Resection Margin of =< 1 mm and Rectal Cancer Recurrence After Sphincter-Preserving Surgery: The Role of a Positive Distal Margin in Rectal Cancer Surgery. *Dis Colon Rectum* **60**, 1175–1183, DOI: 10.1097/DCR.0000000000000900 (2017).
15. Yan, H., Wang, P.-Y., Wu, Y.-C. & Liu, Y.-C. Is a Distal Resection Margin of =< 1 cm Safe in Patients with Intermediate- to Low-Lying Rectal Cancer? A Systematic Review and Meta-Analysis. *J Gastrointest Surg* **26**, 1791–1803, DOI: 10.1007/s11605-022-05342-9 (2022).
16. Manegold, P., Taukert, J., Neeff, H., Fichtner-Feigl, S. & Thomusch, O. The minimum distal resection margin in rectal cancer surgery and its impact on local recurrence - A retrospective cohort analysis. *Int. J. Surg.* **69**, 77–83, DOI: 10.1016/j.ijsu.2019.07.029 (2019).
17. Bhamre, R., Mitra, A., Tamankar, A., Desouza, A. & Saklani, A. Impact of Length of Distal Margin on Outcomes Following Sphincter Preserving Surgery for Middle and Lower Third Rectal Cancers. *Indian J Surg Oncol* **10**, 335–341, DOI: 10.1007/s13193-019-00888-8 (2019).

18. Kazi, M. *et al.* Long-term oncological outcomes of the sphincter preserving total mesorectal excision with varying distal resection margins. *J Surg Oncol* **123**, 1784–1791, DOI: 10.1002/jso.26467 (2021).

19. Arteaga-González, I. *et al.* The Use of Preoperative Endoscopic Tattooing in Laparoscopic Colorectal Cancer Surgery for Endoscopically Advanced Tumors: A Prospective Comparative Clinical Study. *World J. Surg.* **30**, 1658, DOI: 10.1007/s00268-005-0473-3 (2006). _eprint: https://onlinelibrary.wiley.com/doi/pdf/10.1007/s00268-005-0473-3.

20. Yigit, B., Kabul Gurbulak, E. & Ton Eryilmaz, O. Usefulness of Endoscopic Tattooing Before Neoadjuvant Therapy in Patients with Clinical Complete Response in Locally Advanced Rectal Cancer for Providing a Safe Distal Surgical Margin. *J Laparoendosc Adv Surg Tech A* **32**, 506–514, DOI: 10.1089/lap.2021.0382 (2022).

21. Askin, M. P., Waye, J. D., Fiedler, L. & Harpaz, N. Tattoo of colonic neoplasms in 113 patients with a new sterile carbon compound. *Gastrointest Endosc* **56**, 339–342, DOI: 10.1016/s0016-5107(02)70035-7 (2002).

22. Hellmig, S., Stüber, E., Kiehne, K., Kosmahl, M. & Fölsch, U. What do we really know about the long-term safety of colonic tattooing? *Gastrointest Endosc* **61**, 186–187, DOI: 10.1016/s0016-5107(04)02464-2 (2005).

23. Letarte, F. *et al.* Tattooing or not? A review of current practice and outcomes for laparoscopic colonic resection following endoscopy at a tertiary care centre. *Can J Surg* **60**, 394–398, DOI: 10.1503/cjs.004817 (2017).

24. Khoury, W., Abboud, W., Hershkovitz, D. & Duek, S. D. Frozen section examination may facilitate reconstructive surgery for mid and low rectal cancer. *J Surg Oncol* **110**, 997–1001, DOI: 10.1002/jso.23758 (2014).

25. Osako, T. *et al.* Efficacy of intraoperative entire-circumferential frozen section analysis of lumpectomy margins during breast-conserving surgery for breast cancer. *Int J Clin Oncol* **20**, 1093–1101, DOI: 10.1007/s10147-015-0827-2 (2015).

26. Chmielik, E. *et al.* Distal intramural spread of rectal cancer after preoperative radiotherapy: the results of a multicenter randomized clinical study. *Int J Radiat Oncol Biol Phys* **65**, 182–188, DOI: 10.1016/j.ijrobp.2005.11.039 (2006).

27. van der Stel, S. D. *et al.* Size and depth of residual tumor after neoadjuvant chemoradiotherapy in rectal cancer - implications for the development of new imaging modalities for response assessment. *Front Oncol* **13**, 1209732, DOI: 10.3389/fonc.2023.1209732 (2023).

28. Gomes, R. M., Bhandare, M., Desouza, A., Bal, M. & Saklani, A. P. Role of intraoperative frozen section for assessing distal resection margin after anterior resection. *Int J Color. Dis* **30**, 1081–1089, DOI: 10.1007/s00384-015-2244-4 (2015).

29. Heidkamp, J. *et al.* Novel imaging techniques for intraoperative margin assessment in surgical oncology: A systematic review. *Int J Cancer* **149**, 635–645, DOI: 10.1002/ijc.33570 (2021).

30. Giuliani, G. *et al.* Ultrasound assessment of the distal resection margin during robotic rectal surgery. *Color. Dis* **26**, 1741–1746, DOI: 10.1111/codi.17109 (2024).

31. Geldof, F. *et al.* Tumor Segmentation in Colorectal Ultrasound Images Using an Ensemble Transfer Learning Model: Towards Intra-Operative Margin Assessment. *Diagnostics* **13**, 3595, DOI: 10.3390/diagnostics13233595 (2023). Number: 23.

32. Otani, K. *et al.* Usefulness of real-time navigation using intraoperative ultrasonography for rectal cancer resection. *Asian J Endosc Surg* **16**, 819–821, DOI: 10.1111/ases.13242 (2023).

33. Makouei, F. *et al.* Feasibility of a Novel 3D Ultrasound Imaging Technique for Intraoperative Margin Assessment during Tongue Cancer Surgery. *Curr Oncol* **31**, 4414–4431, DOI: 10.3390/curroncol31080330 (2024).

34. Bekedam, N. M. *et al.* Clinical validation of the accuracy of an intra-operative assessment tool using 3D ultrasound compared to histopathology in patients with squamous cell carcinoma of the tongue. *Eur Arch Otorhinolaryngol* **281**, 5455–5463, DOI: 10.1007/s00405-024-08753-3 (2024).

35. Veluponnar, D. *et al.* Toward Intraoperative Margin Assessment Using a Deep Learning-Based Approach for Automatic Tumor Segmentation in Breast Lumpectomy Ultrasound Images. *Cancers (Basel)* **15**, 1652, DOI: 10.3390/cancers15061652 (2023).

36. Almezaien, O. *et al.* The Beneficial Impact of Intraoperative Ultrasound on Resection Margin Status during Breast Conserving Surgery. *Int J Surg Oncol* **2022**, 2268821, DOI: 10.1155/2022/2268821 (2022).

37. de Koning, K. J. *et al.* Feasibility study of ultrasound-guided resection of tongue cancer with immediate specimen examination to improve margin control - Comparison with conventional treatment. *Oral Oncol* **116**, 105249, DOI: 10.1016/j.oraloncology.2021.105249 (2021).

38. Bulbul, M. G. *et al.* The utility of intra-oral ultrasound in improving deep margin clearance of oral tongue cancer resections. *Oral Oncol* **122**, 105512, DOI: 10.1016/j.oraloncology.2021.105512 (2021).

39. Bekedam, N. M. *et al.* Intra-operative resection margin model of tongue carcinoma using 3D reconstructed ultrasound. *Adv. Oral Maxillofac. Surg.* **4**, 100154, DOI: 10.1016/j.adoms.2021.100154 (2021).

40. Layeequr Rahman, R., Puckett, Y., Habrawi, Z. & Crawford, S. A decade of intraoperative ultrasound guided breast conservation for margin negative resection - Radioactive, and magnetic, and Infrared Oh My.... *Am J Surg* **220**, 1410–1416, DOI: 10.1016/j.amjsurg.2020.09.008 (2020).

41. Brouwer de Koning, S. G. *et al.* Ultrasound aids in intraoperative assessment of deep resection margins of squamous cell carcinoma of the tongue. *Br J Oral Maxillofac Surg* **58**, 285–290, DOI: 10.1016/j.bjoms.2019.11.013 (2020).

42. Li, Q.-B. *et al.* In vivo and in situ detection of colorectal cancer using Fourier transform infrared spectroscopy. *World J Gastroenterol* **11**, 327–330, DOI: 10.3748/wjg.v11.i3.327 (2005).

43. Li, S. *et al.* Identification and characterization of colorectal cancer using Raman spectroscopy and feature selection techniques. *Opt Express* **22**, 25895–25908, DOI: 10.1364/OE.22.025895 (2014).

44. Ha, R. *et al.* Optical Coherence Tomography: A Novel Imaging Method for Post-lumpectomy Breast Margin Assessment-A Multi-reader Study. *Acad Radiol* **25**, 279–287, DOI: 10.1016/j.acra.2017.09.018 (2018).

45. Sutton, P. A. *et al.* Fluorescence-guided surgery: comprehensive review. *BJS Open* **7**, zrad049, DOI: 10.1093/bjsopen/zrad049 (2023).

46. Balog, J. *et al.* Intraoperative tissue identification using rapid evaporative ionization mass spectrometry. *Sci Transl Med* **5**, 194ra93, DOI: 10.1126/scitranslmed.3005623 (2013).

47. Georvasili, V. K. *et al.* Detection of cancer cells and tumor margins during colorectal cancer surgery by intraoperative flow cytometry. *Int J Surg* **104**, 106717, DOI: 10.1016/j.ijsu.2022.106717 (2022).

48. Solbakken, A. M. *et al.* Navigation-Assisted Surgery for Locally Advanced Primary and Recurrent Rectal Cancer. *Ann Surg Oncol* **30**, 7602–7611, DOI: 10.1245/s10434-023-13964-9 (2023).

49. Rossberg, N. *et al.* Machine Learning Applications to Diffuse Reflectance Spectroscopy in Optical Diagnosis; A Systematic Review, DOI: 10.48550/arXiv.2503.02905 (2025). ArXiv:2503.02905 [eess].

50. Veluponnar, D. *et al.* Margin assessment during breast conserving surgery using diffuse reflectance spectroscopy. *J. biomedical optics* **29**, 045006–045006 (2024).

51. Veluponnar, D. *et al.* Diffuse reflectance spectroscopy for accurate margin assessment in breast-conserving surgeries: importance of an optimal number of fibers. *Biomed. Opt. Express* **14**, 4017–4036, DOI: 10.1364/BOE.493179 (2023). Publisher: Optica Publishing Group.

52. Geldof, F. *et al.* Toward the use of diffuse reflection spectroscopy for intra-operative tissue discrimination during sarcoma surgery. *J. Biomed. Opt.* **29**, DOI: 10.1117/1.JBO.29.2.027001 (2024).

53. Roode, L. M. d. *et al.* Toward handheld optically guided biopsy combining diffuse reflectance spectroscopy and autofluorescence. *JBO* **30**, 057001, DOI: 10.1117/1.JBO.30.5.057001 (2025).

54. Koning, S. G. B. d. *et al.* Toward complete oral cavity cancer resection using a handheld diffuse reflectance spectroscopy probe. *J. Biomed. Opt.* **23**, 121611, DOI: 10.1117/1.JBO.23.12.121611 (2018). Publisher: SPIE.

55. Harris, K., Rohrbach, D. J., Attwood, K., Qiu, J. & Sunar, U. Optical imaging of tissue obtained by transbronchial biopsies of peripheral lung lesions. *J Thorac Dis* **9**, 1386–1392, DOI: 10.21037/jtd.2017.03.113 (2017).

56. de Roode, L. M. *et al.* Feasibility of diffuse reflection spectroscopy for intraoperative margin assessment during prostatectomy. *Eur. Urol. Open Sci.* **67**, 62–68 (2024).

57. de Roode, L. *et al.* Diffuse reflectance spectroscopy during prostatectomy; towards intraoperative margin assessment. *Eur. Urol.* **85**, S2036–S2037 (2024).

58. Baltussen, E. J. M. *et al.* Using Diffuse Reflectance Spectroscopy to Distinguish Tumor Tissue From Fibrosis in Rectal Cancer Patients as a Guide to Surgery. *Lasers Surg. Medicine* **52**, 604–611, DOI: 10.1002/lsm.23196 (2020).

59. Saito Nogueira, M. *et al.* Evaluation of wavelength ranges and tissue depth probed by diffuse reflectance spectroscopy for colorectal cancer detection. *Sci Rep* **11**, 798, DOI: 10.1038/s41598-020-79517-2 (2021).

60. Fernandes, L. *et al.* Diffuse reflectance and machine learning techniques to differentiate colorectal cancer ex vivo. *Chaos* **31**, 053118, DOI: 10.1063/5.0052088 (2021).

61. Geldof, F., Witteveen, M., Sterenborg, H. J. C. M., Ruers, T. J. M. & Dashtbozorg, B. Diffuse reflection spectroscopy at the fingertip: design and performance of a compact side-firing probe for tissue discrimination during colorectal cancer surgery. *Biomed. Opt. Express* **14**, 128–147, DOI: 10.1364/BOE.476242 (2023). Publisher: Optica Publishing Group.

62. Saito Nogueira, M. *et al.* Diffuse reflectance spectroscopy for colorectal cancer surgical guidance: towards real-time tissue characterization and new biomarkers. *The Analyst* **149**, 88–99, DOI: 10.1039/d3an00261f (2023).

63. Nazarian, S. *et al.* Real-time classification of tumour and non-tumour tissue in colorectal cancer using diffuse reflectance spectroscopy and neural networks to aid margin assessment. *Int. J. Surg. (London, England)* **110**, 1983–1991, DOI: 10.1097/JS9.0000000000001102 (2024).

64. Saito Nogueira, M. *et al.* Insights into Biochemical Sources and Diffuse Reflectance Spectral Features for Colorectal Cancer Detection and Localization. *Cancers* **14**, 5715, DOI: 10.3390/cancers14225715 (2022). Number: 22 Publisher: Multidisciplinary Digital Publishing Institute.

65. Geldof, F., Dashtbozorg, B., Hendriks, B. H. W., Sterenborg, H. J. C. M. & Ruers, T. J. M. Layer thickness prediction and tissue classification in two-layered tissue structures using diffuse reflectance spectroscopy. *Sci. Reports* **12**, 1698, DOI: 10.1038/s41598-022-05751-5 (2022). Publisher: Nature Publishing Group.

66. Baltussen, E. J. M. *et al.* Diffuse reflectance spectroscopy as a tool for real-time tissue assessment during colorectal cancer surgery. *J. Biomed. Opt.* **22**, 1–6, DOI: 10.1117/1.JBO.22.10.106014 (2017).

67. Ehlen, L., Ishizawa, T., Cohen, R. & Chand. Synergy of Fluorescence and Near-Infrared Spectroscopy in Detection of Colorectal Cancer. *J Surg Res* **242**, 349–356 (2019).

68. Imbalanced-learn Developers. SMOTE — Version 0.14.1. Derived from imbalanced-learn.org/stable/references/generated/imblearn.over_sampling.SMOTE.html on 2026-01-22.

69. Chawla, N. V., Bowyer, K. W., Hall, L. O. & Kegelmeyer, W. P. SMOTE: Synthetic Minority Over-sampling Technique. *J. Artif. Intell. Res.* **16**, 321–357, DOI: 10.1613/jair.953 (2002).

70. Baltussen, E. J. M., Sterenborg, H. J. C. M., Ruers, T. J. M. & Dashtbozorg, B. Optimizing algorithm development for tissue classification in colorectal cancer based on diffuse reflectance spectra. *Biomed. Opt. Express, BOE* **10**, 6096–6113, DOI: 10.1364/BOE.10.006096 (2019).

71. Scikit-Learn Team. RBF SVM parameters - scikit-learn 1.8.0 documentation. Derived from scikit-learn.org/stable/auto_examples/svm/plot_rbf_parameters.html on 2026-01-21.

72. Baltussen, E. J. M. *et al.* Tissue diagnosis during colorectal cancer surgery using optical sensing: an in vivo study. *J. Transl. Medicine* **17**, 333, DOI: 10.1186/s12967-019-2083-0 (2019).

Author contributions statement

J.T.H.: Conceptualization, Methodology, Software, Validation, Formal analysis, Investigation, Writing - original draft, Writing - Review & Editing. I.B.: Methodology, Software, Validation, Formal analysis, Investigation, Writing - original draft. A.G.J.A.: Resources, Writing - Review & Editing. B.A.G.: Resources, Writing - Review & Editing. F.G.: Conceptualization, Methodology, Investigation, Writing - Review & Editing. B.D.: Conceptualization, Methodology, Investigation, Writing - Review & Editing, Funding acquisition. T.J.M.R.: Conceptualization, Methodology, Resources, Writing - Review & Editing, Funding acquisition.

Additional information

Correspondence and requests for materials should be addressed to J.T.H. **Competing interests** The authors declare no competing interests. **Funding** Research at the Netherlands Cancer Institute is supported by institutional grants of the Dutch Cancer Society and of the Dutch Ministry of Health, Welfare and Sport.

Table 1. Patient characteristics of complete dataset.

Total	**86**
Gender	Count (%)
Female	46 (53%)
Male	40 (47%)
Neo-adjuvant treatment	Count (%)
None	45 (52%)
Chemotherapy	19 (22%)
Chemo-radiotherapy	16 (19%)
Immunotherapy	4 (5%)
Radiotherapy	2 (2%)
Location of colorectal tumor (*proximal to distal*)	Count (%)
Cecum	8 (9%)
Colon ascendens	12 (14%)
Colon (flexura hepatica)	4 (5%)
Colon transversum	7 (8%)
Colon (flexura lienalis)	4 (5%)
Colon descendens	2 (2%)
Sigmoid	22 (26%)
Rectum	26 (30%)
Other*	1 (1%)
Tumor type	Count (%)
Well/moderately differentiated adenocarcinoma (low grade)	60 (70%)
Poorly differentiated adenocarcinoma (high grade)	11 (13%)
Mucinous adenocarcinoma	11 (13%)
Medullary carcinoma	2 (2%)
No tumor	1 (1%)
Not described	1 (1%)
Mandard Tumor Regression Grade	Count (%)
No pretreatment	46 (53%)
1	1 (1%)
2	5 (6%)
3	14 (16%)
4	16 (19%)
5	3 (3%)
Not mentioned	1 (1%)
pT Stage (*tumor invasion*)	Count (%)
0	1 (1%)
1	0 (0%)
2	7 (8%)
3	49 (57%)
4a	13 (15%)
4b	14 (16%)
Other*	2 (2%)

**peritoneal metastasis*

Table 2. *Performance metrics per combination of model and feature selection method, calculated over five folds.*

Feature Selection (*Model*)	**MCC**	**AUROC**	**Sensitivity**	**Specificity**	**Accuracy**
Linear SVM					
Whole Spectrum	0.75	0.94	0.87	0.86	0.88
First Derivative	0.73	0.93	0.86	0.87	0.87
Linear Discriminant Analysis	0.73	0.93	0.85	0.88	0.87
LASSO	0.75	0.94	0.87	0.88	0.88
k-means Bands	0.64	0.90	0.84	0.80	0.82
Polynomial SVM					
Whole Spectrum	0.72	0.92	0.86	0.86	0.86
First Derivative	0.78	0.95	0.89	0.90	0.89
Linear Discriminant Analysis	0.71	0.93	0.84	0.87	0.86
LASSO	0.72	0.92	0.86	0.87	0.86
k-means Bands	0.68	0.91	0.86	0.82	0.84
RBF SVM					
Whole Spectrum	0.72	0.92	0.86	0.87	0.86
First Derivative	0.78	0.95	0.89	0.90	0.89
Linear Discriminant Analysis	0.72	0.93	0.85	0.87	0.86
LASSO	0.73	0.92	0.86	0.87	0.86
k-means Bands	0.68	0.91	0.87	0.82	0.84
MLP					
Whole Spectrum	0.73	0.93	0.88	0.88	0.87
First Derivative	0.77	0.94	0.85	0.92	0.89
Linear Discriminant Analysis	0.73	0.94	0.86	0.87	0.87
LASSO	0.73	0.93	0.86	0.86	0.86
k-means Bands	0.68	0.90	0.87	0.81	0.84
Random Forest					
Whole Spectrum	0.69	0.92	0.82	0.87	0.85
First Derivative	0.74	0.93	0.86	0.88	0.87
Linear Discriminant Analysis	0.69	0.92	0.82	0.87	0.85
LASSO	0.70	0.92	0.82	0.87	0.85
k-means Bands	0.67	0.92	0.83	0.84	0.84

Supplementary Files

This is a list of supplementary files associated with this preprint. Click to download.

- main.bbl